Materials Today: Proceedings 38 (2021) 1535–1540

Contents lists available at ScienceDirect

Materials Today: Proceedings

journal homepage: www.elsevier.com/locate/matpr

Prediction of strength characteristics of high-entropy alloys Al-Cr-Nb-Ti-V-Zr systems

D.N. Klimenko *, N.Y. Yurchenko, N.D. Stepanov, S.V. Zherebtsov

Laboratory of Bulk Nanostructured Materials, Belgorod State University, Belgorod 308015, Russia

ARTICLE INFO

Article history:
Received 19 June 2020
Accepted 7 August 2020
Available online 9 September 2020

Keywords:
High entropy alloys
Machine learning
Yield strength

ABSTRACT

Experimental evaluations of mechanical properties and investigations microstructure are time-intensive, requiring weeks or months to produce and characterize a small number of candidate alloys. In this work, machine learning approaches were used for prediction yield strengths of high-entropy alloys Al-Cr-Nb-Ti-V-Zr system at 20, 600 and 800 °C. Surrogate prediction model was built with support vector regression algorithm by a dataset including more 30 alloys Al-Cr-Nb-Ti-V-Zr system. Four model alloys were fabricated for testing the surrogate model by vacuum arc melting. After that model alloys were annealed in a quartz tube at 1200 °C 10 h. The microstructure of alloys after heat treatment were investigated with methods of scanning electron microscopy and X-ray structural analysis. Specimens of model alloys were compressed in the air at a nominal strain rate of 10^{-4} s^{-1} at 20, 600 and 800 °C in a universal testing machine to determine the yield strength. The model showed the satisfactory accuracy prediction of yield strengths as single-phase as multi-phase alloys at all test temperatures. In connection with the small size of training dataset accuracy prediction of yield strengths for alloys outside composition space of training dataset is lower than inside.

Selection and peer-review under responsibility of the scientific committee of the International Conference on Modern Trends in Manufacturing Technologies and Equipment 2020.

1. Introduction

Conventional alloys have one principal element, with minor modifications achieved by adding relatively small amounts of other elements. This strategy saves the characteristic properties of the base element and makes this alloy family attractive. Another approach is to use five or more basic elements instead of one for creating high entropy alloy (HEA) – a multicomponent single-phase solid-solution alloy in or near an equiatomic composition [1–3]. But in this case, the number of possible alloy systems is significant increases because the number of HEA systems is a function of N! while the number of conventional alloy systems equals the number of potential elements [4]. In the absence of approaches for the rapid screen of a large number of candidate alloys their investigation takes a lot of time.

Calculating the phase diagram of each candidate alloy using the calculated phase diagram method (for example CALPHAD) [4–7] can help decrease the value of alloys for experimental evaluations. While CALPHAD predictions are reliable over composition ranges for which the databases have been built, but multi-component systems remain largely unexplored.

Surrogate machine learning models successfully use in various fields of modern materials science [8–10] and are promising for enables rapid predictions of mechanical properties and phase composition of HEA. A robust strategy for predicting the formation of a single-phase solid solution HEAs was proposed by Tancret et al. [11]. Their approach based on an assessment of phase formation and a Gaussian process statistical analysis predicted 62 single-phase equimolar HEA. Wen et al. [12] proposed a materials design strategy combining a machine learning (ML) surrogate model with experimental design algorithms to search for high entropy alloys (HEAs) with large hardness in a model Al-Co-Cr-Cu-Fe-Ni system. Their design strategy predicted 35 alloys with hardness values higher than the best value in the training dataset. Amongst these alloys, the hardness of 17 alloys are enhanced by >10% compared to the maximum hardness in our training dataset.

In this work, we use the approach proposed Wen et al for the prediction of yield strengths of alloys Al-Cr-Nb-Ti-V-Zr system in a wide range of temperature.

* Corresponding author.
E-mail address: klimenko@bsu.edu.ru (D.N. Klimenko).

https://doi.org/10.1016/j.matpr.2020.08.145
2214-7853/
Selection and peer-review under responsibility of the scientific committee of the International Conference on Modern Trends in Manufacturing Technologies and Equipment 2020.

2. Materials and methods

In this work, machine learning approaches were used for prediction strength characteristics of high-entropy alloys Al-Cr-Nb-Ti-V-Zr system at room temperature, 600 °C and 800 °C. Dataset for surrogate prediction model included more 30 alloys [13–17].

Alloys of the Al-Cr-Nb-Ti-V-Zr system in a known part of the composition space can be either single-phase or multiphase. Therefore, surrogate prediction model was built with features representing aspects of structure and mechanical properties. List of features and equations for their calculation are provided below.

Difference in atomic radii between elements:

$$\delta = \sqrt{\sum c_i \left(1 - \frac{r_i}{\bar{r}}\right)^2}, \bar{r} = \sum c_i r_i$$

Valence electron concentration:

$$VEC = \sum c_i (VEC)_i$$

Difference in electronegativity between elements:

$$\Delta\chi = \sqrt{\sum c_i \left(\chi_i - \sum c_j \chi_j\right)^2}$$

Mixing enthalpy:

$$H_{mix} = \sum \sum 4\Delta H_{ij}^{mix} c_i c_j$$

Configurational entropy:

$$S_{mix} = -\mathrm{R} \sum c_i \ln(c_i)$$

Work function:

$$\phi = \left(\sum c_i \phi_i\right)^6$$

Shear modulus:

$$\mu = \sum c_i \mu_i$$

Difference in shear modulus:

$$\Delta\mu = \sum c_i \frac{2 \cdot (\mu_i - \mu)}{\mu_i + \mu}$$

γ parameter:

$$= \left(1 - \sqrt{\frac{\left(r_s + \bar{r}\right)^2 - \bar{r}^2}{\left(r_s + \bar{r}\right)^2}}\right) / \left(1 - \sqrt{\frac{\left(r_l + \bar{r}\right)^2 - \bar{r}^2}{\left(r_l + \bar{r}\right)^2}}\right)$$

Λparameter:

$$\Lambda = \frac{\Delta S_{mix}}{\delta^2}$$

Ω parameter:

$$\Omega = \frac{T_m \Delta S_{mix}}{[\Delta H_{mix}]} \qquad T_m = \sum c_i T_i$$

In order to reduce the computation time and improve model robustness by removing the irrelevant and redundant features, we used a correlation analysis. The Pearson correlation coefficient map between different features was built. Pair of features with a correlation coefficient >0.95 were considered as highly correlated and one of these features was excluded from the model.

We employed several well-known machine learning models – including a ridge regression model (rid), a regression tree model (tree), a k-nearest neighbor model (knn) and support vector regression with a linear kernel (svr.lin), a polynomial kernel (svr.poly), and a radial basis function kernel (svr.rbf) for prediction the yield strength of high-entropy alloys Al-Cr-Nb-Ti-V-Zr system.

At the first stage grid search was used for hyperparameter optimization with estimate root mean square error. After that we considered influence of size training dataset on prediction accuracy all used models. Our original dataset was split randomly into a training set and a testing set. The size of training set was between 30 and 90%. Surrogate models were trained with the training sets and were used

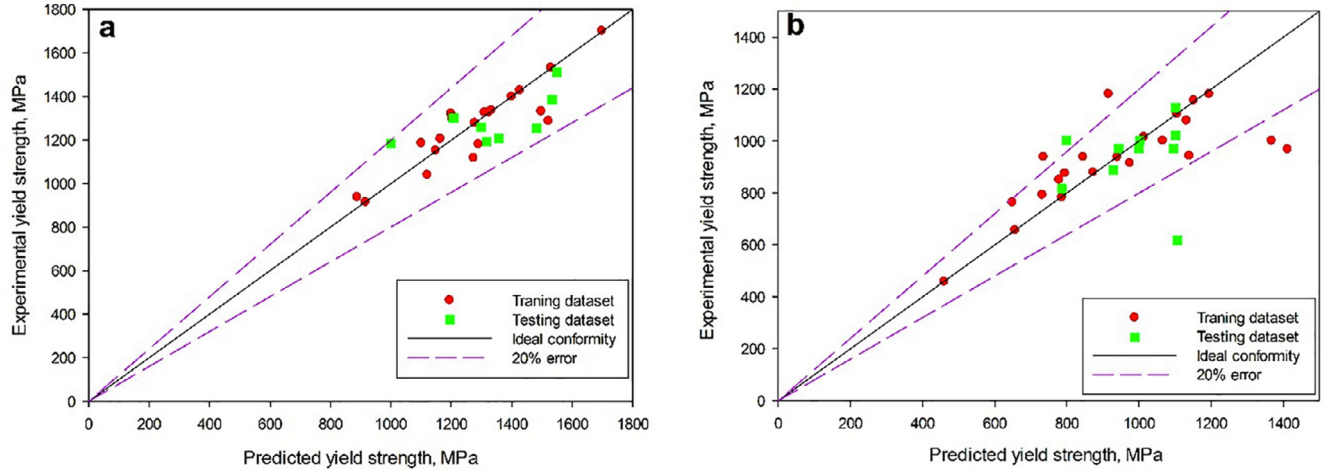

Fig. 1. The experimental and predicted values of yield strength at room temperature (a) and 600 °C (b) for the svr.rbf surrogate model.

Table 1
The compositions of model alloys.

Alloy	Al, % at	Cr, % at	Nb, % at	Ti, % at	V, % at	Zr, % at
$Al_5Cr_5Nb_{38}Ti_{32}V_5Zr_{15}$	5	5	38	32	5	15
$Al_8Cr_{11}Nb_{32}Ti_{20}V_{20}Zr_9$	8	11	32	20	20	9
$A_{l5}Nb_{24}Ti_{40}V_5Zr_{26}$	5	0	24	40	5	26
$Al_4Cr_3Nb_{21}Ti_{40}V_4Zr_{28}$	4	3	21	40	4	28

for prediction yield strengths of the testing set. Obtained values were used for calculation of root mean square error for all machine learning models. The error depends only slightly on the size training dataset for the two model – tree and knn. For other model the error decreases with increasing size of the training set. Optimal size of the training dataset was defined at 70% of full dataset.

The third stage was directed at determining the better model. We employed the bootstrap with replacement and randomly chose 50 training set (size of training set is 70% of full dataset). We trained a model on this bootstrap dataset and made predictions for all the data points in the original training dataset. Obtained values were used for calculation of root mean square error for all machine learning models. The svr.rbf and tree have the minimum prediction error and svr.rbf was chosen as the model to predict yield strengths of HEAs.

Fig. 1 shows comparison predicted and experimental value of yield strengths at room temperature and 600 °C for svr.rbf surrogate model. As can be seen from the Fig. 1, the surrogate model works better for room temperature than for high temperature. We obtained 1000 random 70% training sets for predictions yield strength of model alloys.

3. Experiments and discussion

Model alloys for testing surrogate model were chosen with two methods. In the first approach alloys were chosen with single-phase alloy formation criteria [18]. Grid search alloys system Al – Cr – Nb – Ti – V – Zr was done in the range of concentrations all components 5–50% with step 3%. The number of alloys is satisfied single-phase alloy formation criteria: $\delta < 5.4\%$, $VEC < 6.87$, $\Delta H\_mix = -16.25–4$ kJ/mole, $\Omega > 1.1$, $\varphi > 7$, $\eta > 0.19$ is 221. As model alloys were selected $Al_5Cr_5Nb_{38}Ti_{32}V_5Zr_{15}$, $Al_8Cr_{11}Nb_{32}Ti_{20}V_{20}Zr_9$, $Al_5Nb_{24}Ti_{40}V_5Zr_{26}$ and $Al_4Cr_3Nb_{21}Ti_{40}V_4Zr_{28}$.

The compositions of model alloys are listed in Table 1. Alloys were fabricated by vacuum arc melting only and annealed in a quartz tube at 1200 °C 10 h. After heat treatment alloys were investigated with methods of scanning electron microscopy (Fig. 2) and X-ray structural analysis (Fig. 3a)

As can be seen from Fig. 2a, for the alloys $Al_5Cr_5Nb_{38}Ti_{32}V_5Zr_{15}$, $Al_8Cr_{11}Nb_{32}Ti_{20}V_{20}Zr_9$, $Al_5Nb_{24}Ti_{40}V_5Zr_{26}$ and $Al_4Cr_3Nb_{21}Ti_{40}V_4Zr_{28}$ phase contrast weren't observed. X-ray structural analysis showed only one BCC phase in this alloys. In $Al_8Cr_{11}Nb_{32}Ti_{20}V_{20}Zr_9$ alloy observed three areas with different composition: matrix phase (colored gray in Fig. 2b) and inclusions of Cr-rich (colored dark gray in Fig. 2b) and Zr-rich (colored light gray in Fig. 2b). X-ray structural analysis in this alloy showed BCC phase, Laves phase and phase type Zr_5Al_3.

For compression test 6x6x9 mm specimens were cut off after annealing at 1200 °C 10 h. Yield strengths was determined at 20, 600 and 800 °C with universal testing machine Instron 300LX-B1-C3-J1C, strain rate $1 \cdot 10^{-4}$ s^{-1}. Engineering curves of compression tests of samples were showed in Fig. 3.

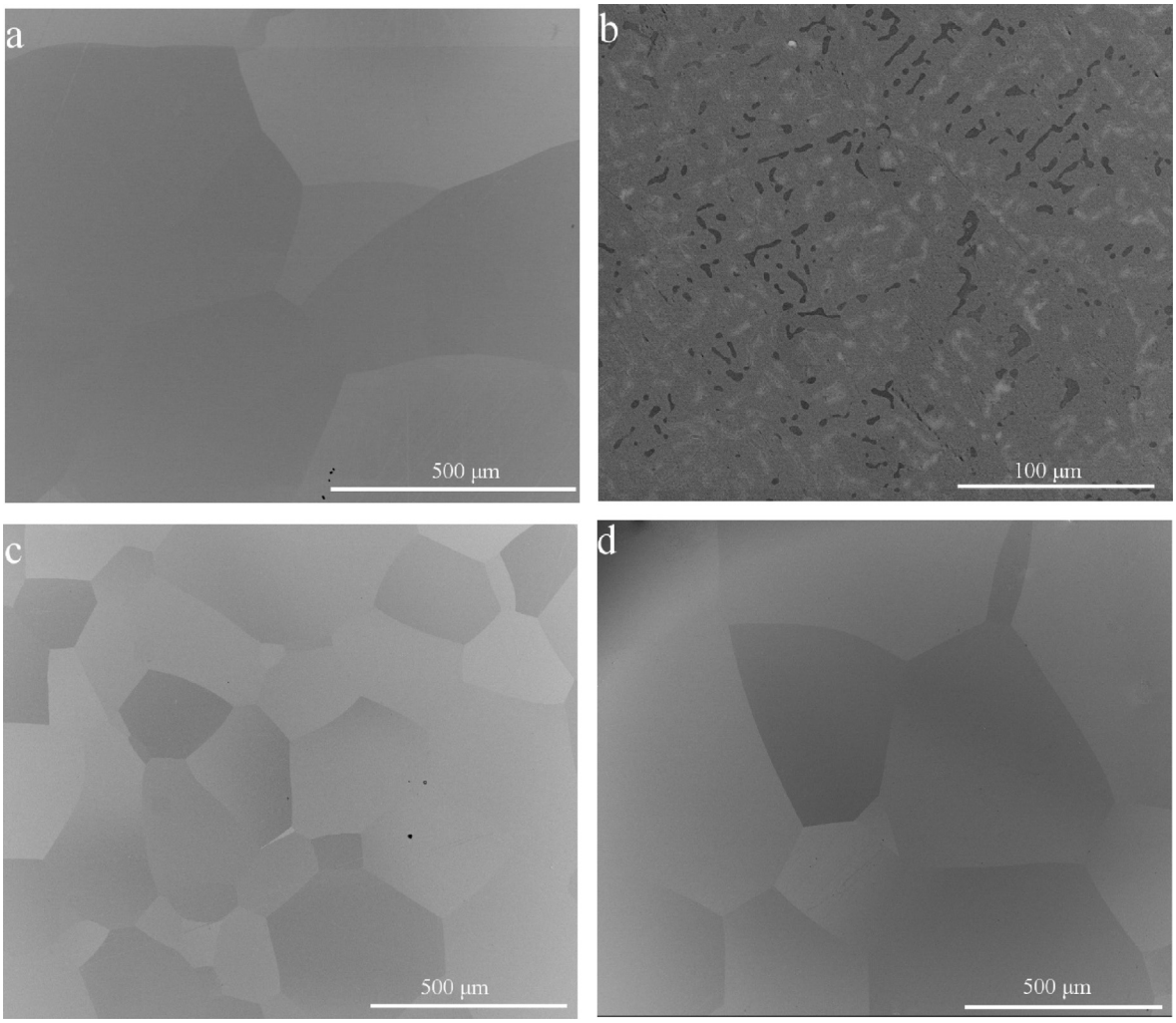

Fig. 2. Microstructure of model alloys after annealing at 1200 °C 10 h $Al_5Cr_5Nb_{38}Ti_{32}V_5Zr_{15}$ (a), $Al_8Cr_{11}Nb_{32}Ti_{20}V_{20}Zr_9$ (b), $Al_5Nb_{24}Ti_{40}V_5Zr_{26}$ (c) and $Al_4Cr_3Nb_{21}Ti_{40}V_4Zr_{28}$ (d).

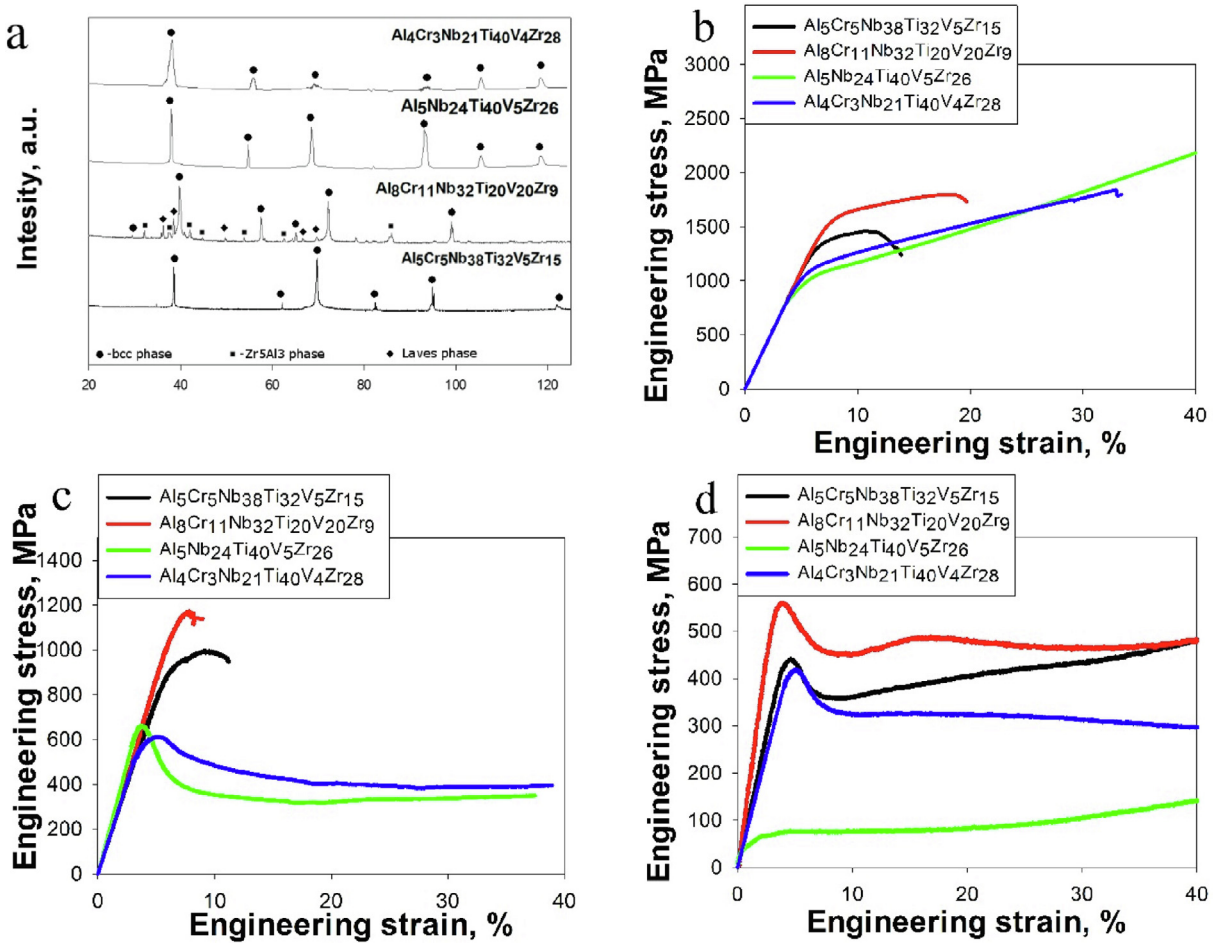

Fig. 3. Engineering curves of compression tests of model alloys at room temperature (a), 600 °C (b) and 800 °C (c).

Table 2
Predicted and experimental value of yield strength at room temperature and 600 °C.

Alloy	σ_{YS} at 20 °C, MPa	σ_{YS} predicted at 20 °C, MPa	σ_{YS} at 600 °C, MPa	σ_{YS} predicted at 600 °C, MPa	σ_{YS} at 800 °C, MPa	σ_{YS} predicted at 800 °C, MPa
$Al_5Cr_5Nb_{38}Ti_{32}V_5Zr_{15}$	1215	1232	845	837	420	448
$Al_8Cr_{11}Nb_{32}Ti_{20}V_{20}Zr_9$	1425	1459	1065	1015	525	581
$A_{l5}Nb_{24}Ti_{40}V_5Zr_{26}$	880	1162	616	796	880	1162
$Al_4Cr_3Nb_{21}Ti_{40}V_4Zr_{28}$	940	1243	511	826	405	415

$Al_8Cr_{11}Nb_{32}Ti_{20}V_{20}Zr_9$ alloy demonstrates the highest strength over the entire temperature range of tests and low ductility at 20 and 600 °C. $Al_5Cr_5Nb_{38}Ti_{32}V_5Zr_{15}$ alloy shown similar behavior and less strength. $Al_5Nb_{24}Ti_{40}V_5Zr_{26}$ alloy demonstrates good ductility over the entire temperature range of tests and well strength at 800 °C. In contrast, $Al_4Cr_3Nb_{21}Ti_{40}V_4Zr_{28}$ alloy shown extremal low strength at 800 °C.

Predicted and experimental value of yield strength for model alloys at testing temperatures are submitted in Table 2.

Comparison of predicted and experimental value of yield strength for model alloys at testing temperatures are shown in Fig. 4.

The accuracy prediction of yield strengths for $Al_5Cr_5Nb_{38}Ti_{32}V_5Zr_{15}$ and $Al_8Cr_{11}Nb_{32}Ti_{20}V_{20}Zr_9$ alloys is quite high at all test temperatures. For $Al_5Nb_{24}Ti_{40}V_5Zr_{26}$ alloy prediction errors is much higher at 20 and 600 °C, but for at 800 °C it is much lower. The accuracy prediction of yield strength for $Al_4Cr_3Nb_{21}Ti_{40}V_4Zr_{28}$ alloy is the smallest at all test temperatures.

In the Fig. 4b–d shows predicted and experimental value of yield strength for model alloys and the largest and smallest yield strength values in the training dataset for each temperature studied. The distribution of yield strength values in the training dataset is similar to normal distribution. Because the size of the training dataset is quite small the number of alloys near its boundaries is not enough for high accuracy prediction. For $Al_5Cr_5Nb_{38}Ti_{32}V_5Zr_{15}$ and $Al_8Cr_{11}Nb_{32}Ti_{20}V_{20}Zr_9$ alloys yield strengths is well predicted at all test temperatures because their values near the center of the training dataset. The yield strength of $Al_5Nb_{24}Ti_{40}V_5Zr_{26}$ is well predicted at 800 °C and much worse predicted at other temperatures when its yield strength near boundary of training dataset.

4. Conclusion

Surrogate model for predict yield strength for alloys of AlCrNbTiVZr system at 20, 600 and 800 °C was built. The model showed the satisfactory accuracy prediction of yield strengths as single-

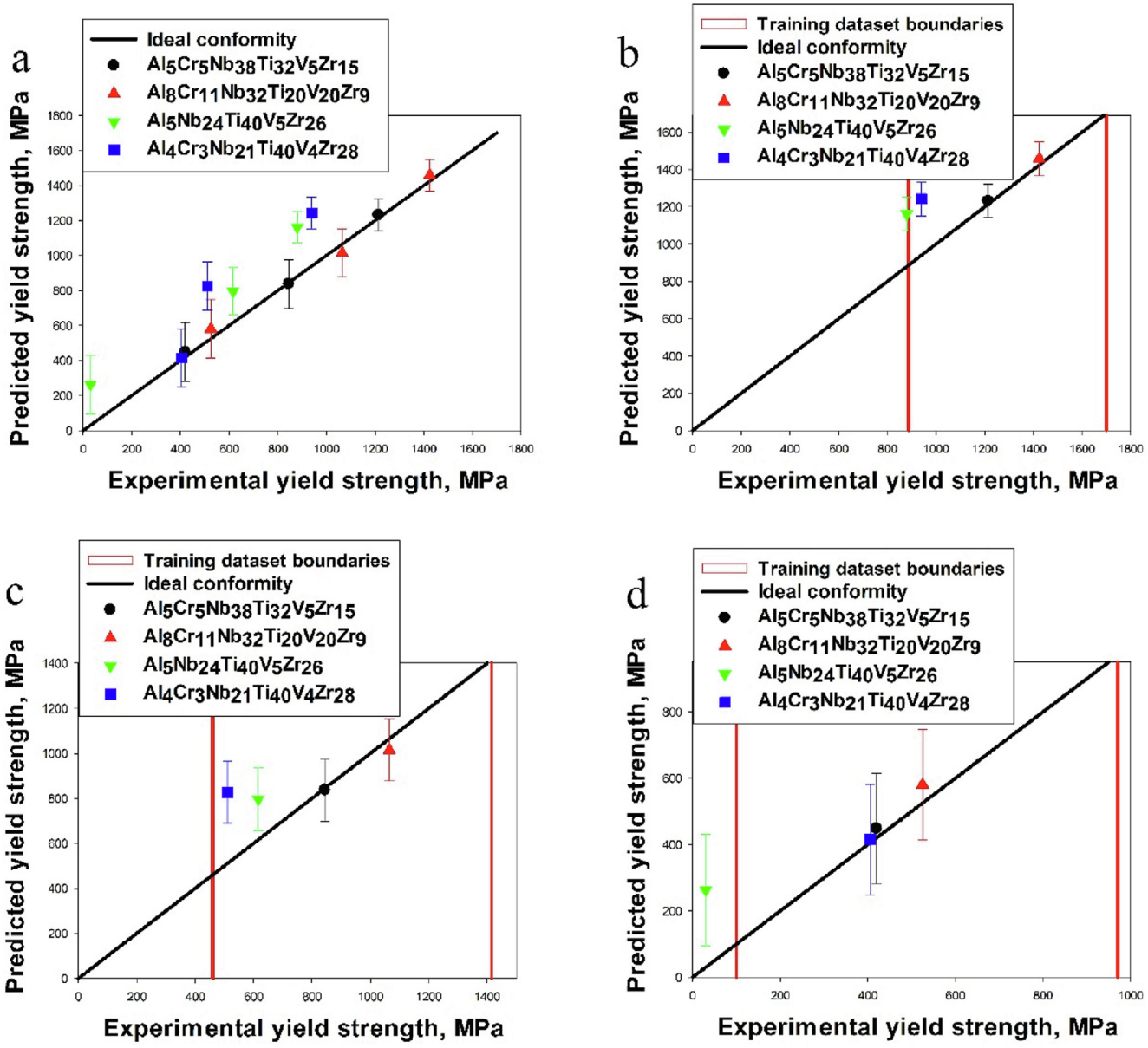

Fig. 4. Predicted and experimental value of yield strength for model alloys at all testing temperatures (a), at room temperature (b), 600 °C (c) and 800 °C (d) with training dataset boundaries.

phase as multi-phase alloys at all test temperatures. In connection with small size of training dataset accuracy prediction of yield strengths for alloys outside composition space of training dataset is lower than inside.

CRediT authorship contribution statement

D.N. Klimenko: Software, Investigation, Conceptualization. **N.Y. Yurchenko:** Validation, Investigation. **N.D. Stepanov:** Writing - review & editing. **S.V. Zherebtsov:** Supervision.

Declaration of Competing Interest

The authors declare that they have no known competing financial interests or personal relationships that could have appeared to influence the work reported in this paper.

Acknowledgement

This study was supported by Russian Science Foundation, grant № 19-79-30066.

References

[1] J.W. Yeh, JOM 65 (2013) 1759–1771.
[2] Y. Zhang, T.T. Zuo, Z. Tang, M.C. Gao, K.A. Dahmen, P.K. Liaw, Prog. Mater Sci. 61 (2014) 1–93.
[3] M.H. Tsai, J.W. Yeh, Mater. Res. Lett. 2 (2014) 107–123.
[4] O.N. Senkov, J.D. Miller, D.B. Miracle, C. Woodward, Calphad 50 (2015) 32–48.
[5] J.M. Sanchez, I. Vicario, J. Albizuri, T. Guraya, J.C. Garcia, J. Mater. Res. Technol. 8 (2019) 795–803.
[6] A.J.S.F. Tapia, D. Yim, H.S. Kim, B.J. Lee, Intermetallics 101 (2018) 56–63.
[7] C. Zhang, F. Zhang, S. Chen, W. Cao, JOM 64 (2012) 839–845.
[8] R. Ramprasad, R. Batra, G. Pilania, A. Mannodi-Kanakkithodi, C. Kim, NPJ Comput. Mater. 3 (2017) 1–13.
[9] D. Xue, P.V. Balachandran, J. Hogden, J. Theiler, D. Xue, T. Lookman, Nature Commun. 7 (2016) 11241.

[10] Y.T. Sun, H.Y. Bai, M.Z. Li, W.H. Wang, J. Phys. Chem. Lett. 14 (2017) 3434–3439.
[11] F. Tancret, I. Toda-Caraballo, E. Menou, P.E.J.R. Díaz-Del, Mater. Des. 115 (2017) 486–497.
[12] C. Wen, Y. Zhang, C. Wang, D. Xue, Y. Bai, S. Antonov, Y. Su, Acta Mater. 170 (2019) 109–117.
[13] J.P. Couzinié, O.N. Senkov, D.B. Miracle, G. Dirras, Data Brief 21 (2018) 1622–1641.
[14] N.D. Stepanov, N.Y. Yurchenko, E.S. Panina, M.A. Tikhonovsky, S.V. Zherebtsov, Mater. Lett. 188 (2017) 162–164.
[15] N.D. Stepanov, N.Y. Yurchenko, D.V. Skibin, M.A. Tikhonovsky, G.A. Salishchev, J. Alloy. Compd. 652 (2015) 266–280.
[16] N.D. Stepanov, D.G. Shaysultanov, G.A. Salishchev, M.A. Tikhonovsky, Mater. Lett. 142 (2015) 153–155.
[17] M.C. Gao, C. Zhang, P. Gao, F. Zhang, L.Z. Ouyang, M. Widom, J.A. Hawk, Solid State Mater. Sci. 21 (2017) 238–251.